COMMUNICATION

A bis-vanadyl coordination complex as a two-qubit quantum gate

Ivana Borilovic,[a] Pablo J. Alonso,[b] Olivier Roubeau [b] and Guillem Aromí [a,c,*]

Received 00th January 20xx,
Accepted 00th January 20xx

DOI: 10.1039/x0xx00000x

A new bis-hydroxyphenylpyrazolyl ligand, H_4L, allows to isolate and structurally characterize vanadyl and titanyl analogues of dinuclear complexes $(Bu_4N)_2[(MO)_2(HL)_2]$ (M=V,Ti). The weak dipolar coupling and relatively short quantum coherence determined for the divanadyl anion are optimal for a two-qubit molecular architecture proposed to implement electron-mediated nucelar quantum simulations.

One of the most pursued scientific goals is the realization of quantum computing,[1] which uses the laws and resources of quantum mechanics to implement fast very complex algorithms,[2-4] realize quantum simulations[5] or exploit quantum cryptography.[6] This requires a two-level quantum system as the elementary unit of information (qubit) and a technology to address these qubits in logical ways and interconnect them for computation. Among the proposed systems for realizing qubits,[7-10] the molecular electronic spin is especially attractive for chemists.[11-13] Thus, important efforts have been made to understand the factors controlling the quantum coherence of the spin in transition metal[14-16] and lanthanide coordination complexes.[17-19] The realization of quantum gates requires the coherent manipulation of several inter-connected qubits. Molecules have been prepared as prototypes of 2qubit quantum gates, either as dimers of inequivalent entangled metal ions,[20, 21] or as metal-based pairs of qubits with a switchable interaction.[22, 23] It has also been suggested to use the nuclear spin degrees of freedom as *N*-qudits (units of information of dimension *N*),[24, 25] and some schemes rely on the hyperfine interaction between the nuclear and electronic spins for the implementation of elaborate protocols, such as quantum error correction methods[26] or the realization of the Grover algorithm.[27] A recent report puts forward a coordination anion containing two weakly coupled vanadyl centres, each exhibiting hyperfine coupling between its electronic spin (S = 1/2) and its nuclear magnetic moment (I = 7/2).[28] The characteristics of this molecule were used to simulate the theoretical implementation of a 2qubit scheme with both qubits encoded by two m_I states of each nuclear spin (specifically, $|0\rangle = |5/2\rangle$ and $|1\rangle = |7/2\rangle$). A switchable interaction between both qubits and their entanglement is ensured by the coupling between the electronic spin moments through the hyperfine coupling at each metal. Thus, the interaction between both electronic spins makes any inversion of these spins using microwaves dependent on the nuclear spin, which allows the implementation of a conditional 2qubit gate. The lack of a single crystal X-ray structure however limits a detailed description of this gate, while the qubit separation and associated spin-spin interaction may need to be optimized. Thus, this important development urgently requires the access to model qugate systems allowing exact correlations of their performance with their metric parameters and also enabling to study the isolated gates inside a diamagnetic matrix.

We report here the synthesis and structure of a novel bis-hydroxyphenylpyrazolyl ligand, H_4L, causing the formation of vanadyl and titanyl containing complexes $(Bu_4N)_2[(VO)_2(HL)_2]$ (**1**) and $(Bu_4N)_2[(TiO)_2(HL)_2]$ (**2**), respectively, together with a solid solution of **1** within a matrix of **2**, termed **3**. Thus, the potential performance of **1** as 2qubit quantum gate has been evaluated by magnetometry and continuous and pulsed EPR in the bulk and diluted within a solid-state diamagnetic matrix.

Ligand H_4L was conceived as a possible entry into dinuclear complexes with two separate weakly interacting metals, thanks to two spaced chelating pockets (Fig. 1).

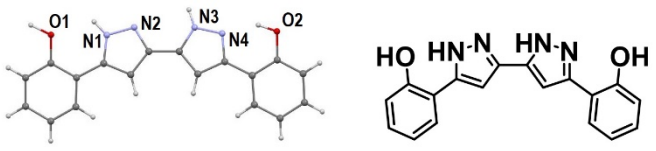

Figure 1. Ligand H_4L and representation of its molecular structure.

[a] Departament de Química Inorgànica i Orgànica, Universitat de Barcelona, Diagonal 645, 08028 Barcelona, Spain. E-mail: guillem.aromi.qi.ub.es.
[b] Instituto de Ciencia de Materiales de Aragón (ICMA), CSIC and Universidad de Zaragoza, Plaza San Francisco s/n, 50009, Zaragoza, Spain
[c] Institut of Nanoscience and Nanotechnology of the University of Barcelona (IN2UB), Barcelona, Spain.

† Footnotes relating to the title and/or authors should appear here.
Electronic Supplementary Information (ESI) available: [details of any supplementary information available should be included here]. See DOI: 10.1039/x0xx00000x

It was prepared *via* the double ring closure of adjacent β-diketone units with hydrazine, on the precursor molecule 1,6-bis-(2-hydroxyphenyl)-1,3,4,6-hexanetetraone (H_4L1; Fig. S1). H_4L1 was synthesized through a Claisen condensation between two equivalents of 2-hydroxyacetophenone and one equivalent of dimethyl oxalate (Figs. S1 to S3). H_4L crystallizes from the reaction mixture in the monoclinic *C*2/c space group with half a molecule of hydrazine, in the form of pairs of almost flat H_4L molecules disposed parallel, face-to-face, and connected through hydrogen bonds (Tables S1 and S3, Figs. S4-S6). H_4L was then recrystallized from acetone, deprotonated with Bu_4NOH in pyridine and made to react with $VOSO_4$ (Eq. 1), producing crystals of **1** upon diffusion of Et_2O to the reaction mixture.

$$2\ H_4L + 6\ Bu_4NOH + 2\ VOSO_4 \rightarrow$$
$$\rightarrow (Bu_4N)_2[(VO)_2(HL)_2] + 2\ (Bu_4N)_2SO_4 + 6\ H_2O \quad (1)$$

The analogous reaction using $TiO(acac)_2$ leads to the formation of **2,** as colorless crystals. The molecular structure of both complexes was established by SCXRD (see below). Their integrity in solution was corroborated by mass spectrometry (MS, Fig. S7). In view of this, a solid solution of **1**, diluted within a diamagnetic matrix of compound **2**, was obtained by dissolving in pyridine crystals of the $(VO)^{2+}$ and $(TiO)^{2+}$ complexes in the 1:4 molar ratio. Diffusion of Et_2O into this mixture caused the crystallization of the doped system **3**, analyzed by SCXRD (see below) with formulation close to $(Bu_4N)_2[(VO)_2(HL)_2]_{0.20}[(TiO)_2(HL)_2]_{0.80}$. Complexes **1** and **2** crystallize in the triclinic space group $P\bar{1}$ and $P2_1/n$, respectively. Interestingly, the space group of **3** is the same as that of **1**, as if the minor component of the solution were acting as template for the mode of crystallization. The unit cell of **1** contains two crystallographically inequivalent $[(VO)_2(HL)_2]^{2-}$ complex anions, almost identical to each other (Fig. 2). Four tetrabutylammonium cations and nine solvate pyridine molecules complete the unit cell content, while the asymmetric unit consists of half this composition. The asymmetric unit of **2** comprises one half $[(TiO)_2(HL)_2]^{2-}$ complex and one Bu_4N^+ cation, with four of these present in the unit cell. Complexes $[(VO)_2(HL)_2]^{2-}$ and $[(TiO)_2(HL)_2]^{2-}$ are very similar, both well represented by Fig. 2, and will be described together. They contain two flat HL^{3-} ligands, parallel and facing each other, linked by their coordination to two V(IV)/Ti(IV) metals. The latter are chelated at their equatorial sites and bridged by the HL^{3-} donors, which keep them (hereafter in the **1**/**2** format) 8.267/8.538 Å (in average for **1**) apart. The coordination of all the metals is squared pyramidal by virtue of the oxo groups at one of both apical positions of each metal. Within each complex, these oxo groups are mutually *trans* (*i.e.* pointing to opposite sides of the molecular plane). The average equatorial M–O and M–N bond distances are, respectively, 1.928/1.906 and 2.089/2.182 Å. A larger affinity for oxygen than for nitrogen is reflected in these distances, which is more evident for Ti(IV) than for V(IV). The M=O separations are 1.601/1.644 Å. The effect of the oxo group causes a separation of the metals from the equatorial planes, with distances of 0.536/0.510 Å. The shortest intermolecular metal–metal distance is 9.025/7.188 Å. Despite the planarity of the complex anions and their aromatic rings, the lattices of **1** and **2** do not show π···π interactions. In **1**, the complexes are arranged with the same orientation, approximately as layers that alternate with layers of Bu_4N^+ cations, with pyridine molecules accommodated within the voids (Fig. S7). In **2**, the structure is much more compact, given the lack of pyridine, and the complexes exhibit two orientations (Fig. S8). The arrangement of the molecules in **3** is analogous to the organization in **1**.

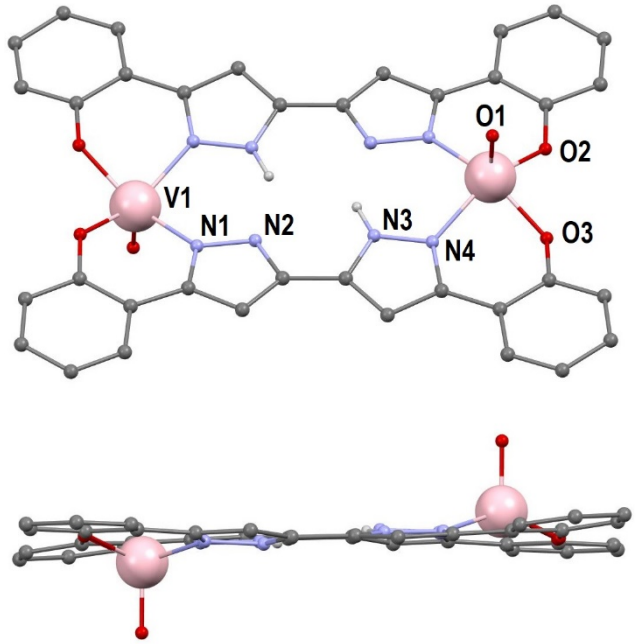

Fig. 2. Top and side views of the molecular structure of the anion $[(VO)_2(HL)_2]^{2-}$ of **1**. Unique heteroatoms labelled. C atoms in grey. Only H atoms on N atoms shown.

To evaluate the potential of the vanadyl pairs in the $[(VO)_2(HL)_2]^{2-}$ complex anion as a 2-qubit architecture, the bulk magnetic properties of **1** were first examined. The temperature dependence of χT, χ being the molar magnetic susceptibility, is well reproduced with a Curie-Weiss model with C = 0.7398 cm^3mol^{-1} (corresponding to g = 1.973) and θ = –0.07 K (Fig. S9), thus in line with a paramagnet with only very weak antiferromagnetic interactions. The magnetization *vs.* field data at 2 K virtually follows the Brillouin function for 2 isolated S = 1/2 spins with g = 1.98, thus also supporting the presence of only very weak interactions. Considering the similar intra- and inter-molecular V···V separations and the absence of clear exchange-coupling pathway(s), the most likely origin of these is through-space dipolar interaction, either intra- and/or inter-molecular. On the other hand, the solid-state continuous-wave (CW) EPR spectra of **1** and **3** are quite similar, except for the sharper lines in the case of magnetically dilute **3** (Figure S10). The spectrum of **3** is consistent with hyperfine coupled vanadyl species that are in addition weakly interacting with each other. This and the similarity of the spectra for the pure and diluted systems **1** and **3** support the presence of weak magnetic interactions within the molecular

$[(VO)_2(HL)_2]^{2-}$ complex, one of the requirements for the proposed 2-qubit scheme.[28]

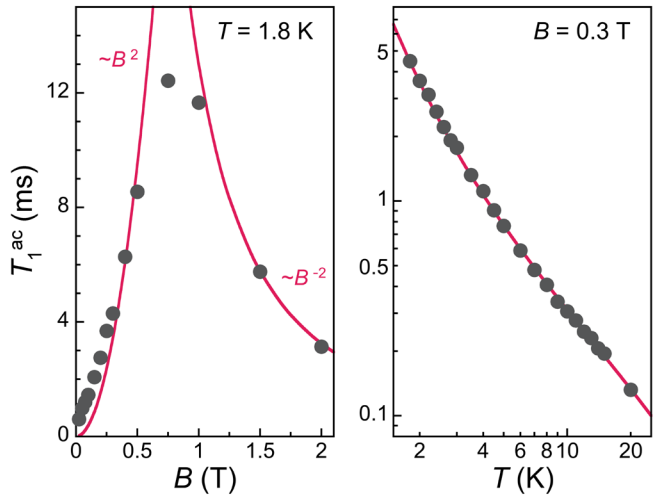

Fig. 3. Left: spin-lattice relaxation time T_1^{ac} as a function of the *dc* magnetic field *B* at 1.8 K for **1** (grey symbols). The red lines represent B^2 and B^{-2} dependences, as indicated. Right: temperature dependence of T_1^{ac} at 0.3 T applied *dc* fields (grey symbols). The red line is a fit of the expression $T_1^{ac\ -1} = aB^2T + cT^m$ to the data (see text).

The spin dynamics of the $[(VO)_2(HL)_2]^{2-}$ species were first evaluated through *ac* susceptibility measurements, in determining the spin-lattice relaxation time T_1^{ac} of **1**. While no out-of-phase component of the susceptibility is detected in zero-field at 1.8 K, applying a *dc* field as low as 25 mT is sufficient to bring the maximum of the out-of-phase component, which defines the characteristic time of the magnetization relaxation, in the experimental frequency window. At low fields, T_1^{ac} increases to reach about 12 ms at 0.75 T, and then decreases markedly above 1 T (Fig. 3 left). The low-field increase is found to be ≈ B^2 and originates in the growing *dc* field overcoming spin-spin and spin-nucleus interactions, these being at the origin of the two-phonon spin relaxation processes by breaking the degeneracy of the Kramers doublet. The fast decrease at higher fields corresponds to the direct relaxation process, typically dominant at high fields, due to its strong field dependence, and expected to be ≈B^{-4} for a Kramers system. Here, the dependence is closer to a B^{-2} dependence, which is an indication of phonon bottleneck effects, expected for magnetically concentrated solids.[29] The temperature dependence of T_1^{ac} was determined up to 20 K at 0.3 T, exhibiting the expected decrease due to thermally-activated relaxation processes (Fig. 3 right). The temperature dependence is however fairly weak, close behaving as $T^{-1.3}$, thus confirming the presence of strong phonon bottleneck effects.[29, 30] A good simulation of the temperature dependence was obtained considering direct, Orbach and Raman relaxation processes through the expression $(T_1^{ac})^{-1} = aB^2T + b\Delta/[\exp(\Delta/T)-1] + cT^n$, with a = 343(50) $s^{-1}K^{-1}$, b = 22(2) $s^{-1}K^{-3}$, c = 0.08(2) $s^{-1}K^{-3}$, and the Orbach gap and Raman exponent fixed at Δ = 4 K and n = 3, respectively. The direct process is only relevant at the lowest temperatures, while the Raman process remains dominant at higher temperatures. Both are found to be of the same order as in the monometallic $[VO(dbm)_2]$ molecule.[15] The Orbach-type relaxation is necessary to reproduce correctly the lower temperature range < 5 K, and can reasonably be ascribed to interactions among the vanadyl spins, also surfacing in this temperature range in the χT *vs.* T data, and providing the necessary excited state. Overall, the observed fairly long spin relaxation times should not harm reasonably long coherence times T_M, while the field and temperature dependences of T_1^{ac} are in line with those previously observed in other S = 1/2 systems portrayed as molecular qubits.[15, 31]

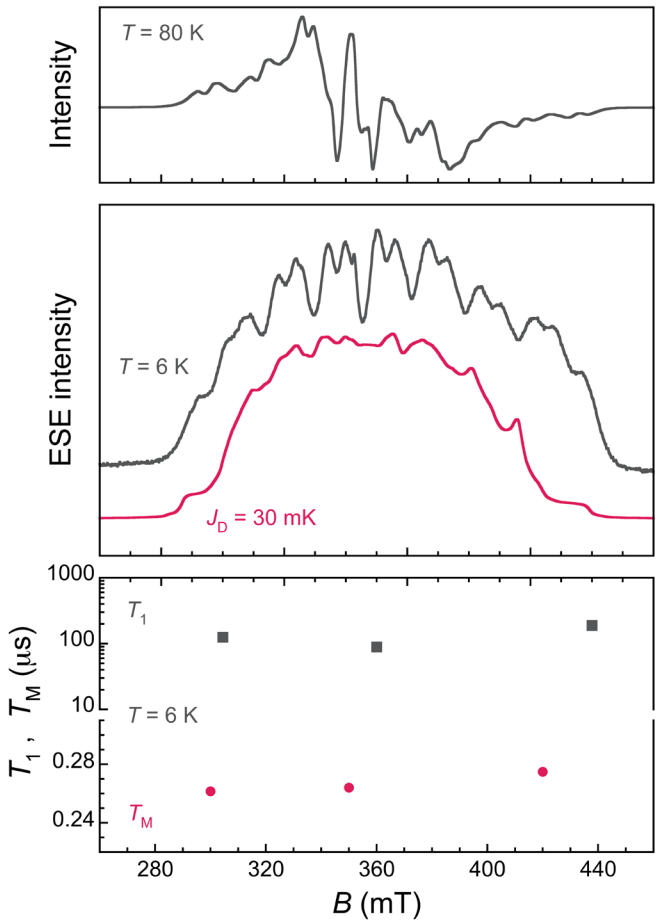

Fig. 4. Top: CW-EPR spectrum of **3** at 80 K. Middle: ESE-detected 2p EPR spectrum of **3** at 6 K (top grey trace, average of spectra with τ = 140 and 200 ns) and its simulation (bottom red trace) with a spin Hamiltonian contemplating two equivalent axial vanadyl coupled through a dipolar interaction with J_D = 30 mK (see ESI for details). Bottom: mean longitudinal relaxation time T_1 and phase memory time T_M for **3** at 6 K and three different magnetic fields (see ESI for details).

Pulsed-EPR was used to evaluate the presence of quantum coherence in **3**. At low temperature, a rather strong electron spin-echo (ESE) signal is detected at any field in the range 280-430, thus consistent with the CW-EPR spectrum, and confirming that the vanadyl pairs exhibit a measurable quantum coherence. Using a 2-pulse Hahn echo detection, a well-resolved ESE-detected EPR spectrum was determined for **3** at 6 K. The latter was again characteristic of a weakly-interacting system with a complex set of lines likely resulting

from the combination of splitting processes caused by both hyperfine spin-nuclei (S=1/2 and I=7/2 for $^{51}V^{IV}$, which has a natural abundance of 99.76%) and spin-spin interactions (Fig. 4). Attempts of simulating the spectrum were done considering the later coupling to be either purely dipolar, exchange-coupled isotropic or planar (see ESI for details). Neither exchange-coupled models reproduce the features of the experimental spectrum (Figs. S13-S14), while the best simulation is obtained using a dipolar interaction of the order of 30 mK (Figs. 4 and S15), confirming the assumption that the dipolar interaction is the most relevant in **1**. The estimated interaction is about one order of magnitude larger than in the divanadyl anion originally proposed for a 2-qubit architecture, $[PPh_4][(VO)_2(L)_2]$ (**4**, L = tetranion of a dicatechol Schiff base ligand).[28] The difference can reasonably be ascribed to the change in V···V separation, shorter by about 2 Å in **1**/**3** than in **4**, which shows ability to tune the inter-qubit interaction designing the synthesis. The spin-lattice relaxation time T_1 and the phase memory time T_M at 6 K of **3** were estimated at three different magnetic fields through inversion recovery and echo decay experiments, respectively (Fig. 4 bottom, see ESI for details). The mean spin-lattice relaxation is found to be of the order of 90-190 μs in **3**, in reasonable agreement with values derived by *ac* susceptibility for **1**. The about 50 times shorter T_1 with respect to a dilute frozen solution of **4** can be still ascribed to the expected effect of magnetic dilution, since **3** remains a rather concentrated magnetic system considering its dilution level of approximately 20%. The phase-memory time T_M of the vanadyl spins in **3** appears to be basically constant at 0.26-0.27 μs over the field range studied, thus about four times shorter than for the dilute frozen solution of **4**.[28] This remains however remarkable considering the concentrated nature of the sample, and the shortcomings caused by the close proximity of the two vanadyl electronic spins in the $[(VO)_2(HL)_2]^{2-}$ complex. It must be emphasized here that in the proposed scheme, the electron spin is not embodying the qubit, in fact, its function requiring a relatively fast decoherence. Indeed, the dephasing of the electronic spins is only relevant for the electron-mediated implementation of fast ($\leq$ 150 ns) 2-qubit gates, so that the dephasing time in **3** appears to be optimal.

Conclusions

Through the adequate design of a bis-chelating ligand, we have prepared and structurally characterized a complex anion featuring two vanadyl moieties in the adequate separation to favour a weak though significant through-space dipolar interaction, necessary to realize a proposed two-qubit molecular architecture. The spin dephasing time of the divanadyl complex anion has been determined in the solid-state thanks to the ability to dilute it in its titanyl diamagnetic analogue, and found to be optimal for the implementation of the proposed computation scheme.

Conflicts of interest

There are no conflicts to declare.

Notes and references

1. M. A. Nielsen and I. L. Chuang, *Quantum Computation and Quantum Information*, Cambridge University Press, 2000.
2. D. Deutsch and R. Jozsa, *Proceedings of the Royal Society of London Series a-Mathematical Physical and Engineering Sciences*, 1992, **439**, 553-558.
3. P. W. Shor, *Siam Journal on Computing*, 1997, **26**, 1484-1509.
4. L. K. Grover, *Phys. Rev. Lett.*, 1997, **79**, 325-328.
5. I. M. Georgescu, S. Ashhab and F. Nori, *Reviews of Modern Physics*, 2014, **86**, 153-185.
6. N. Lütkenhaus and A. J. Shields, *New Journal of Physics*, 2009, **11**, 045005.
7. T. D. Ladd, F. Jelezko, R. Laflamme, Y. Nakamura, C. Monroe and J. L. O'Brien, *Nature*, 2010, **464**, 45-53.
8. M. H. Devoret and R. J. Schoelkopf, *Science*, 2013, **339**, 1169-1174.
9. C. Monroe and J. Kim, *Science*, 2013, **339**, 1164-1169.
10. T. H. Taminiau, J. Cramer, T. van der Sar, V. V. Dobrovitski and R. Hanson, *Nat. Nanotechnol.*, 2014, **9**, 171-176.
11. A. Ardavan, O. Rival, J. J. L. Morton, S. J. Blundell, A. M. Tyryshkin, G. A. Timco and R. E. P. Winpenny, *Phys. Rev. Lett.*, 2007, **98**, 057201.
12. G. Aromí, D. Aguilà, P. Gamez, F. Luis and O. Roubeau, *Chem. Soc. Rev.*, 2012, **41**, 537-546.
13. A. Gaita-Ariño, F. Luis, S. Hill and E. Coronado, *Nature Chem.*, 2019, **11**, 301-309.
14. K. Bader, D. Dengler, S. Lenz, B. Endeward, S.-D. Jiang, P. Neugebauer and J. Van Slageren, *Nature Commun.*, 2014, **5**, 5304.
15. M. Atzori, E. Morra, L. Tesi, A. Albino, M. Chiesa, L. Sorace and R. Sessoli, *J. Am. Chem. Soc.*, 2016, **138**, 11234-11244.
16. M. S. Fataftah, J. M. Zadrozny, S. C. Coste, M. J. Graham, D. M. Rogers and D. E. Freedman, *J. Am. Chem. Soc.*, 2016, **138**, 1344-1348.
17. M. J. Martinez-Perez, S. Cardona-Serra, C. Schlegel, F. Moro, P. J. Alonso, H. Prima-Garcia, J. M. Clemente-Juan, M. Evangelisti, A. Gaita-Arino, J. Sese, J. van Slageren, E. Coronado and F. Luis, *Phys. Rev. Lett.*, 2012, **108**, 247213.
18. M. D. Jenkins, Y. Duan, B. Diosdado, J. J. Garcia-Ripoll, A. Gaita-Arino, C. Gimenez-Saiz, P. J. Alonso, E. Coronado and F. Luis, *Physical Review B*, 2017, **95**, 8.
19. K. S. Pedersen, A.-M. Ariciu, S. McAdams, H. Weihe, J. Bendix, F. Tuna and S. Piligkos, *J. Am. Chem. Soc.*, 2016, **138**, 5801-5804.
20. D. Aguilà, L. A. Barrios, V. Velasco, O. Roubeau, A. Repollés, P. J. Alonso, J. Sesé, S. J. Teat, F. Luis and G. Aromí, *J. Am. Chem. Soc.*, 2014, **136**, 14215-14222.
21. F. Luis, A. Repolles, M. J. Martinez-Perez, D. Aguila, O. Roubeau, D. Zueco, P. J. Alonso, M. Evangelisti, A. Camon, J. Sese, L. A. Barrios and G. Aromi, *Phys. Rev. Lett.*, 2011, **107**.
22. J. Salinas-Uber, M. Estrader, J. Garcia, P. Lloyd-Williams, A. Sadurni, D. Dengler, J. van Slageren, N. F. Chilton, O. Roubeau, S. J. Teat, J. Ribas-Arino and G. Aromi, *Chem., Eur. J.*, 2017, **23**, 13648-13659.
23. J. Ferrando-Soria, E. Moreno Pineda, A. Chiesa, A. Fernandez, S. A. Magee, S. Carretta, P. Santini, I. J.

Vitorica-Yrezabal, F. Tuna, G. A. Timco, E. J. L. McInnes and R. E. P. Winpenny, *Nature Commun.*, 2016, **7**, 11377.
24. E. Moreno-Pineda, M. Damjanović, O. Fuhr, W. Wernsdorfer and M. Ruben, *Angewandte Chemie International Edition*, 2017, **56**, 9915-9919.
25. S. Thiele, F. Balestro, R. Ballou, S. Klyatskaya, M. Ruben and W. Wernsdorfer, *Science*, 2014, **344**, 1135-1138.
26. R. Hussain, G. Allodi, A. Chiesa, E. Garlatti, D. Mitcov, A. Konstantatos, K. S. Pedersen, R. De Renzi, S. Piligkos and S. Carretta, *J. Am. Chem. Soc.*, 2018, **140**, 9814-9818.
27. C. Godfrin, A. Ferhat, R. Ballou, S. Klyatskaya, M. Ruben, W. Wernsdorfer and F. Balestro, *Phys. Rev. Lett.*, 2017, **119**, 187702.
28. M. Atzori, A. Chiesa, E. Morra, M. Chiesa, L. Sorace, S. Carretta and R. Sessoli, *Chem. Sci.*, 2018, **9**, 6183-6192.
29. J. Soeteman, A. J. van Duyneveldt, C. L. M. Pouw and W. Breur, *Physica*, 1973, **66**, 63-69.
30. S. Gómez-Coca, A. Urtizberea, E. Cremades, P. J. Alonso, A. Camón, E. Ruiz and F. Luis, *Nature Commun.*, 2014, **5**, 4300.
31. A. Urtizberea, E. Natividad, P. J. Alonso, M. A. Andrés, I. Gascón, M. Goldmann and O. Roubeau, *Adv. Funct. Mater.*, 2018, **28**, 1801695.

1